Amide Proton Transfer (APT) Imaging of Human Brain Tumors with B0 Inhomogeneity Correction

J. Zhou[1,2], J. Blakeley[3], J. Hua[1,2], M. Kim[1,2], and P. C. van Zijl[1,2]

[1]Neurosection, Division of MR Research, Department of Radiology, Johns Hopkins University, Baltimore, MD, United States, [2]F.M. Kirby Research Center for Functional Brain Imaging, KKI, Baltimore, MD, United States, [3]Department of Neurology, Johns Hopkins University, Baltimore, MD, United States

Introduction: APT imaging (1,2) is a kind of CEST imaging (3-5), in which the contrast is determined by a change in bulk water intensity due to chemical exchange with saturated amide protons of endogenous mobile proteins and peptides. It provides a unique protein-based MRI contrast for imaging of brain tumors and other human diseases. For MRI, shimming and RF frequency settings are often based on the NMR signal from a whole volume or tissue (e.g., a head). Each voxel in the imaging slice may have a somewhat different frequency offset. Therefore, a potential problem that arises from field inhomogeneity is a shift of CEST-spectrum for some local regions of interest with respect to the water frequency for the whole volume. Because the human brain is large, B_0 inhomogeneity poses a significant problem for human APT imaging. It has been shown (1) that the B_0 inhomogeneity can be corrected on a pixel-by-pixel basis using curve fitting to a complete CEST spectrum (usually with 20-40 offsets). However, the resulting APT images are generally noisy, unless more time is taken to increase the number of acquisition. In this study, we present a practical method to acquire high-SNR APT images with the acceptable scanning time.

Materials and Methods: *MRI acquisition.* Experiments were performed on a Philips 3T MRI scanner using a body coil for RF transmission and an 8-channel SENSE coil for reception. RF saturation power and time were 3 μT and 500 ms, respectively. Other imaging parameters were TR 3 sec, TE 30 ms, matrix 128×128, FOV 230×230 mm^2, and slice thickness 5 mm. Higher-order shimming was employed. High-SNR APT-weighted images were acquired with six offsets (±3, ±3.5, ±4 ppm) and 8 averages (Fig. 1). In an extra scan, a CEST spectrum was acquired (33 offsets from 8 to -8 ppm in the interval of 0.5 ppm, one average). The total scanning time for these two scans was about **5 min**. Eight brain tumor patients were recruited. All patients provided written informed consent as required.

Data analysis. (i) The MT ratio (MTR) is defined as: MTR = 1 – S_{sat}/S_0. The APT signal can be separated out through asymmetry analysis of the MT data about the water frequency, i.e., through an MTR asymmetry parameter: $MTR_{asym}(3.5ppm) = S_{sat}(-3.5ppm)/S_0 - S_{sat}(+3.5ppm)/S_0$. (ii) The CEST spectrum with 33 offsets was fitted through all offsets using a 12th-order polynomial on a pixel-by-pixel basis. After this, the fitted curve was interpolated using an offset resolution of 1 Hz (namely, 2048 points). The actual water resonance was assumed to be at the frequency with the lowest signal intensity. The shift values of frequency formed a map of water center frequency offsets in units of Hz. (iii) To correct for the field inhomogeneity effects on high-SNR APT images, the acquired APT data for offsets (+4, +3.5, +3 ppm; namely, +512, +448, +384 Hz) for each pixel were interpolated (and extended) to 257 points (576, 575, …, 320; namely, +4.5 to +2.5ppm) and shifted correspondingly along the direction of the offset axis using the fitted central frequency map. A similar procedure was applied to the negative-offset data (-3, -3.5, -4 ppm). (iv) Finally, the **uncorrected and corrected high-SNR APT images** were calculated, respectively, according to the uncorrected and corrected APT data of two central offsets ±3.5 ppm. B_0 field inhomogeneities less than ±128 Hz could be corrected using this procedure.

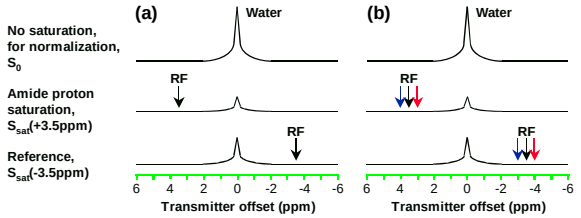

Fig. 1. Two schemes to acquire high-SNR APTw images. (a) Standard two-offset APT scan (+3.5 ppm for label, -3.5 ppm for reference). (b) New six-offset APT scan (±3, ±3.5, ±4 ppm).

Results and Discussion: Fig. 2 (top row) shows acquired MR imaging for a patient with a grade III oligodendroglioma. Three large red spots in the uncorrected APTw image are the result of a susceptibility artifact near air-tissue interfaces (sinus, ear), which could be corrected by the six-offset APT technique. The hyperintense area on the corrected APTw image is much smaller than the abnormal area on FLAIR, but larger than that on the Gd-T1w image. Hence, APT imaging shows a tumor appearance unique from conventional MRI. Fig. 2 (lower row) demonstrates APT imaging of a pathologically confirmed low-grade oligodendroglioma in a 26-year-old woman. Again, the B_0 inhomogeneity-induced artifact is clearly visible in the uncorrected two-offset APTw image. It can be seen that the FLAIR image highlights an abnormal tumor area, but no visible signal enhancement is found on both the corrected APTw and Gd-T1w image. Fig. 3 shows a quantitative analysis on the corrected APT images from all of eight patients. The APT imaging intensity in low-grade gliomas is lower and there is greater APT enhancement with increasing tumor grade. This is consistent with increasing mobile protein concentrations in high-grade tumors measured previously by others (6) using single-voxel MRS.

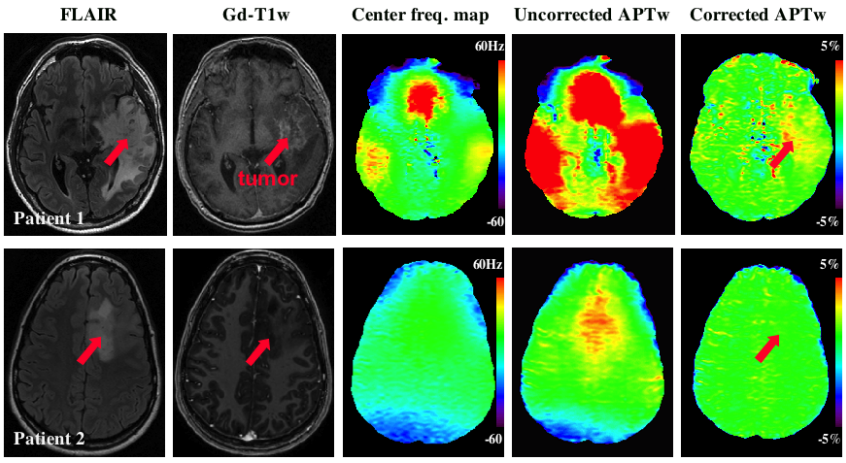

Fig. 2 (left). APT-weighted images compared with other types of MRI. Patient 1: grade III oligodendroglioma. Patient 2: Low-grade oligodendroglioma.

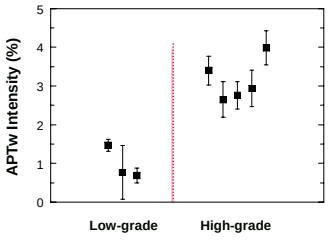

Fig. 3. APTw signal intensity as a function of brain tumor grade. High grade: grade III & IV. n = 8.

Conclusions: We demonstrated a practical six-offset method that, in combination with a full CEST reference spectrum, was able to correct for the artifacts caused by B_0 inhomogeneity on human brain APT images. Early results suggest that APT may provide unique imaging features in gliomas.

References: (1) Zhou et al. Nature Med. 2003;**9**:1085. (2) Jones et al. MRM 2006;**56**:585. (3) Ward et al. JMR 2000;**143**:79. (4) Zhang et al. JACS 2001;**123**:1517. (5) Aime et al. MRM 2002;**47**:639. (6) Howe et al. MRM 2003;**49**:223. **Grant Support:** NIH-NCRR P41015241; Dana Foundation.